JOC The Journal of Organic Chemistry

Article

pubs.acs.org/joc

Snapshot of Oxidation of Thiolate by Diiodine: Stabilization of Intermediate by NH···S Hydrogen Bonds

Taka-aki Okamura,* Toshihisa Kaga, Satoshi Yamashita, Ryosuke Furuya, and Kiyotaka Onitsuka

Department of Macromolecular Science, Graduate School of Science, Osaka University, Toyonaka, Osaka 560-0043, Japan

Supporting Information

ABSTRACT: Ordinary thiolate (RS^-) reacts with diiodine (I_2) to afford an intermediate sulfenyl iodide (RSI) by releasing I^-; RSI is readily converted to disulfide (RSSR) by a disproportionation reaction. In the case of thiolate Ar^1S^- containing very bulky acylamino groups forming NH···S hydrogen bonds, the crystal of the intermediate, $[Ar^1S{-}I{-}I]^-$, was obtained under usual conditions, and the structure was determined by X-ray diffraction analysis. The results show that the intramolecular NH···S hydrogen bonds stabilized the intermediate $[Ar^1S{-}I{-}I]^-$, consistent with theoretical calculations.

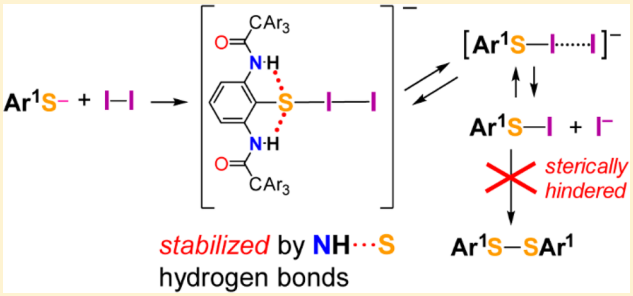

INTRODUCTION

The oxidation of thiol (RSH) with diiodine is a well-known reaction that affords disulfide via intermediate sulfenyl iodide (RSI), as shown in eqs 1−3. The reaction mechanism was originally proposed for the stable RSI groups of cysteine residues in proteins in aqueous media,[1] whereas simple small RSI molecules are decomposed to disulfide by disproportionation in the solution even at a low temperature (eq 3).[2]

$$RSH + I_2 \rightarrow RSI + HI \quad (1)$$

$$RSI + RSH \rightarrow RSSR + HI \quad (2)$$

$$2RSI \rightarrow RSSR + I_2 \quad (3)$$

The undesirable strong acid, HI, can be neutralized with an alkaline solution; however, it promotes the overoxidation of RSI to sulfinic acid (RSO_2H).[3,4] Generally, a tertiary amine or metal salts in organic solvent are used in this reaction.[5] Eqs 1 and 2 can be rewritten as eqs 4 and 5 using thiolate anion (RS^-).

$$RS^- + I_2 \rightarrow RSI + I^- \quad (4)$$

$$RSI + RS^- \rightarrow RSSR + I^- \quad (5)$$

Goto and Okazaki group reported a sufficiently robust RSI, BmtSI (see Supporting Information (SI)), as the first example.[6] The adequately bulky substituent groups sterically hindered the formation of disulfide bond.

Bulky ligands are useful in bioinorganic chemistry to realize the active site and hydrophobic environment of metalloenzymes. We recently developed novel ligands containing bulky hydrophobic acylamino groups ($(4\text{-}t\text{-}BuC_6H_4)_3CCONH$ = Ar_3CCONH) and synthesized model compounds of enzymes.[7−9] These compounds formed intramolecular NH···X (X = O, S) hydrogen bonds and exhibited good solubility in nonpolar solvents, e.g., toluene, thus elucidating the regulating mechanism of the activity at the active site of enzymes.

During the synthesis of a newly designed ligand Ar^1S^- (Figure 1), we accidentally obtained a crystal structure of the

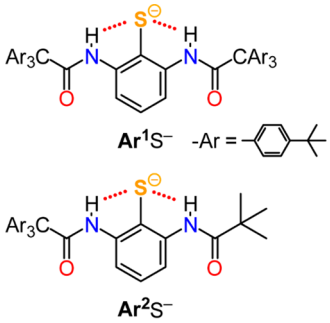

Figure 1. Thiolates containing NH···S hydrogen bonds.

intermediate in the oxidation of thiolate with diiodine. As shown in Figure 2a, the intermediate $[Ar^1S{-}I{-}I]^-$ was crystallized with sulfenyl iodide $Ar^1S{-}I$ forming $[Ar^1S{-}I{\cdots}I{-}I{-}SAr^1]^-$ linkage. The structure of $[RS{-}I{-}I]^-$ or $RS{-}I{\cdots}I^-$ is just like the snapshot of the intermediate releasing I^- anion in an S_N2-type reaction shown in eq 4. Two X-ray crystal structures of pure Ar^1SI and $[Ar^1SI_2]^-$ were also successfully obtained.

RESULTS AND DISCUSSION

Synthesis. The acyl group (Ar_3CCO) is too bulky to acylate the fourth amino group of bis(2,6-diaminophenyl) disulfide, even though bis[2,6-di(triphenylacetylamino)phenyl] disulfide has been synthesized by a general procedure.[10] Once the trisubstituted compound was isolated, the final amino group was converted to a less bulky pivaloylamino group (Scheme 1).

Received: January 22, 2017
Published: February 1, 2017

DOI: 10.1021/acs.joc.7b00160
J. Org. Chem. 2017, 82, 2187−2192

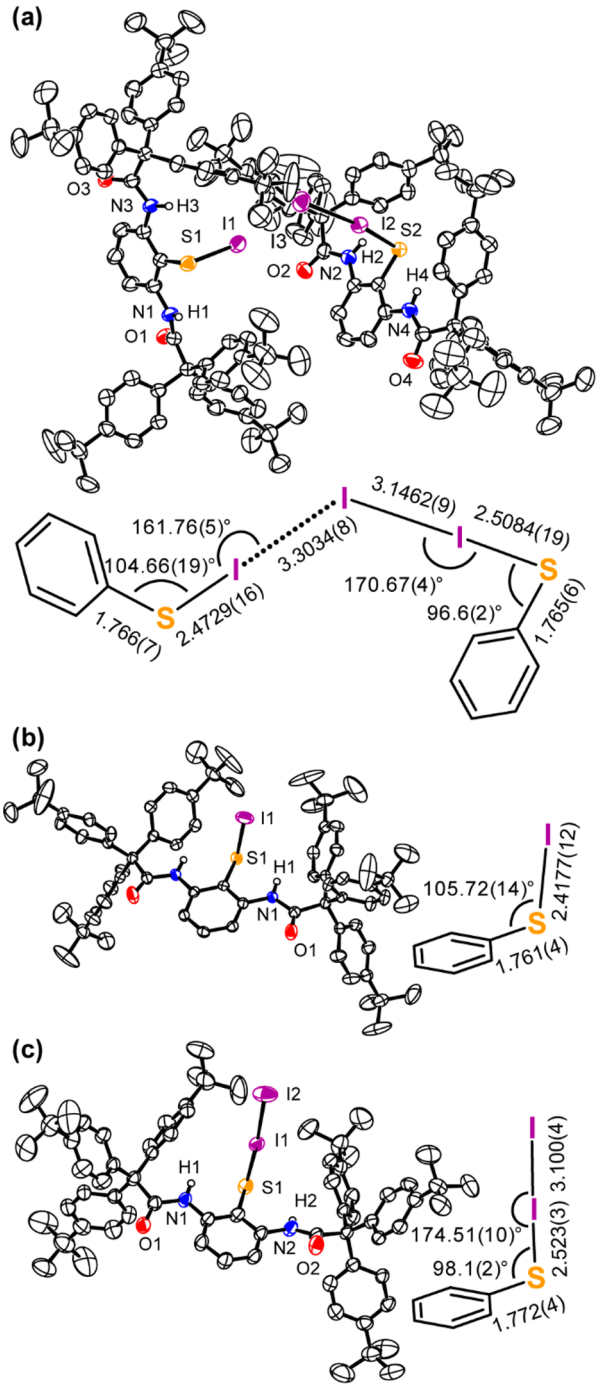

Figure 2. Molecular structures of (a) the anion part of $(NEt_4)[\mathbf{Ar^1}SI{\cdot}I_2S\mathbf{Ar^1}]$, (b) $\mathbf{Ar^1}SI$, and (c) the anion part of $(NEt_4)[\mathbf{Ar^1}SI_2]$. The schematic drawings indicate selected bond distances (Å) and angles (deg) along with short contacts I···I⁻.

The resulting unsymmetrical disulfide $\mathbf{Ar^1}S{-}S\mathbf{Ar^2}$ was reduced with NEt_4BH_4 in a mixture of toluene and ethanol. Only $(NEt_4)[\mathbf{Ar^1}S]$ precipitated as a colorless powder, and $(NEt_4)[\mathbf{Ar^2}S]$ remained in the solution due to significantly different solubility (Scheme 2, Figure 1). The corresponding potassium salts were obtained by a similar method using KBH_4.

$(NEt_4)[\mathbf{Ar^1}S]$ was completely characterized; this compound was crystallized from a suitable solvent containing a small amount of acetonitrile, affording colorless blocks of $(NEt_4)[\mathbf{Ar^1}S]{\cdot}1.75(CH_3CN)$. The structure was determined by X-ray

Scheme 1. Synthetic Route of the Disulfides[a]

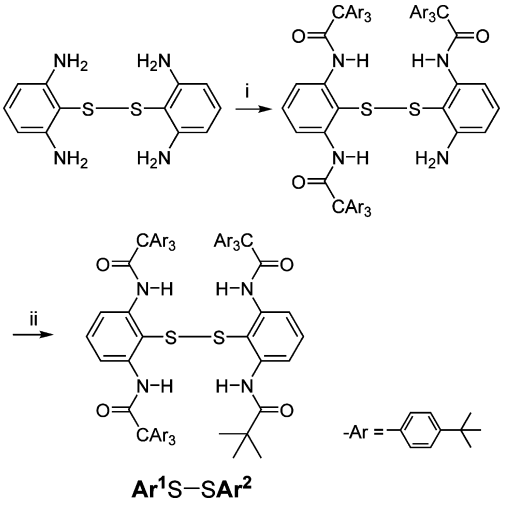

[a](i) Ar_3CCOCl, NEt_3/CH_2Cl_2, reflux. (ii) *t*-BuCOCl, NEt_3/CH_2Cl_2, reflux.

Scheme 2. Preparation of the Thiolate Anion and Oxidation by Diiodine[a]

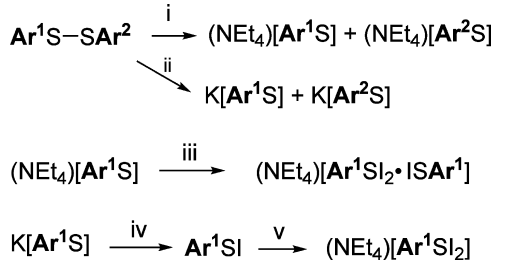

[a](i) NEt_4BH_4 in toluene/EtOH. (ii) KBH_4 in toluene/EtOH. (iii) I_2/toluene. (iv) I_2 in toluene/CH_3CN. (v) $NEt_4I/CHCl_3$.

diffraction analysis (Table S1 and Figure S1).[11] The slightly shorter C–S distance (1.750(4) Å) than normal values (1.77–1.79 Å) in diaryl disulfides[10] indicates that the negative charge or lone pair of electrons on the sulfur atom are delocalized on the adjacent aromatic carbon, increasing the C═S double bond character. Similar tendencies are found in the reported structures of arenethiolates.[12]

To synthesize the disulfide $\mathbf{Ar^1}S{-}S\mathbf{Ar^1}$, $(NEt_4)[\mathbf{Ar^1}S]$ was oxidized with diiodine in toluene. A soluble part in toluene was collected and crystallized. The recrystallization of the product afforded reddish orange blocks suitable for X-ray diffraction analysis. The determined X-ray structure is shown in Figure 2a. Surprisingly, $[\mathbf{Ar^1}S{-}I{-}I]^-$ and $\mathbf{Ar^1}SI$ forming $[\mathbf{Ar^1}S{-}I{\cdots}I{-}I{-}S\mathbf{Ar^1}]^-$ array were observed, just like the snapshots during a nucleophilic attack of $\mathbf{Ar^1}S^-$ anion to I_2 producing $\mathbf{Ar^1}SI$ and releasing I^- anion (eqs 4 and 6). The product $\mathbf{Ar^1}SI$ was recombined with the I^- ion to form $[\mathbf{Ar^1}SI_2]^-$ (eq 7).

$$[\mathbf{Ar^1}S]^- + I_2 \rightarrow [\mathbf{Ar^1}S - I - I]^- \rightarrow [\mathbf{Ar^1}S - I{\cdots}I]^- \rightarrow \mathbf{Ar^1}SI + I^- \quad (6)$$

$$\mathbf{Ar^1}SI + I^- \rightarrow [\mathbf{Ar^1}SI_2]^- \quad (7)$$

The sulfenyl iodide $\mathbf{Ar^1}SI$ was quantitatively obtained from the reaction of $K[\mathbf{Ar^1}S]$ with equimolar diiodine along with the precipitates of insoluble KI in a mixture of toluene and

DOI: 10.1021/acs.joc.7b00160
J. Org. Chem. 2017, 82, 2187–2192

acetonitrile (Scheme 2). The recrystallization from 1,2-dimethoxyethane (DME) afforded orange plates of $\mathbf{Ar^1}$SI·DME. The X-ray crystal structure is shown in Figures 2b and S2a. The two oxygen atoms of DME chelated to the terminal iodine forming O···I contacts, indicating that the terminal I has electron-deficient $I^{\delta+}$ character. The sulfenyl iodide is considerably stable such as the reported stable sulfenyl iodides,[6,13] and the disproportionation to disulfide (eq 3) never occurred. $\mathbf{Ar^1}$SI is stabilized by the bulky Ar_3CCONH groups that completely cover the sulfur atoms to prevent them from forming disulfide bonds.

Isolation and Properties of $(NEt_4)[\mathbf{Ar^1}SI_2]$. The ^{1}H NMR spectrum of $\mathbf{Ar^1}$SI in $CDCl_3$ is shown in Figure S3a. The addition of NEt_4I shifted the NH and aromatic proton signals depending on the amount of NEt_4I, which converged to certain chemical shifts. In these spectra, only one set of signals was observed, indicating the presence of a fast exchange equilibrium on the NMR time scale. The gradual evaporation of a 1:1 mixture of $\mathbf{Ar^1}$SI and NEt_4I in chloroform afforded the adduct $(NEt_4)[\mathbf{Ar^1}SI_2]$ in a reasonable yield (Scheme 2). ^{1}H NMR spectra of $(NEt_4)[\mathbf{Ar^1}SI_2]$ in $CDCl_3$ showed clear dependence on the concentration, indicating the equilibrium with the dissociation constant of 1.0×10^{-3}M (Figures S4 and S5). The X-ray crystal structure is shown in Figure 2c. The intermolecular CH···I (2.78—3.15 Å) and CH···S (2.95 Å) hydrogen bonds with chloroform and NEt_4^+ cation are shown in Figure S2b. The presence of NH···S hydrogen bonds (2.53 and 2.60 Å) was also confirmed. Because the bulky substituents could not cover the terminal iodine atom, the stabilization of S−I−I bond was probably caused by electronic factors.

NH···S Hydrogen Bonds. The strength of NH···S hydrogen was estimated by IR spectra using the established method.[7] The ν(NH) values were listed in Table 1 along with

Table 1. IR and ^{1}H NMR Spectroscopic Data for the Amide NH Groups

	IR in the solid state		^{1}H NMR in $CDCl_3$
	ν(NH)/cm^{-1}	$\Delta\nu$(NH)[a]	δ(NH)/ppm
$(NEt_4)[\mathbf{Ar^1}S]$	3201	−202	10.03
$[\mathbf{Ar^1}SI]$	3329	−74	8.96
$(NEt_4)[\mathbf{Ar^1}SI_2]$	3288	−115	9.13 (9.22[b])

[a]Difference from the value (3403 cm^{-1}) for the free amide NH group of $Ar_3CCONHPh$ in solution (10 mM in CH_2Cl_2).[7] [b]The estimated value for the true NH signal of $(NEt_4)[\mathbf{Ar^1}SI_2]$ without dissociation from the plot in Figure S5.

the ^{1}H NMR chemical shifts of NH signals. The negative shift of ν(NH), $\Delta\nu$(NH), indicates the strength of the hydrogen bond in the order $(NEt_4)[\mathbf{Ar^1}S] > (NEt_4)[\mathbf{Ar^1}SI_2] > [\mathbf{Ar^1}SI]$, which is consistent with the order of the downfield shifts of NH signals in ^{1}H NMR spectra.

S−I−I Bonds. The selected bond distances (Å) and angles (deg) are shown in Figure 2 and listed in Table S2 along with the data of the related compounds. The geometrical parameters are significantly different from the reported values. Several C−S−I−I bonds have been reported for charge-transfer (CT) complexes of thiones,[14] including thiourea,[15] imidazole-2-thiones,[16] and thioamides,[17] or thioether[18] with diiodine. To the best of our knowledge, such a CT complex with I_2 has not yet been reported for thiolates.[19] In the case of the thioether, the longest I−I distance was 2.816(2) Å, and the shortest S−I distance was 2.760(6) Å.[18] This indicates a significant longer distance than the free I−I distance (2.715(6) Å) of diiodine in the solid state,[20] but the difference was small. In the case of thione, most compounds contain the adjacent electron-rich N atom. The most typical compound is $\mathbf{L^1}$=S−I−I where $\mathbf{L^1}$ is *N*-heterocyclic carbene (Table S2).[17] The N atoms stabilized the electron-deficient carbon atom in the polarized $C^{\delta+}-S-I\cdots I^{\delta-}$ structure. The C−S distance is significantly short (1.706(2) Å) for a normal arenethiolate,[12] reflecting the double-bond character. The formation of an S−I bond (2.6981(7) Å) weakened the I−I bond (2.8662(6) Å).

In $(NEt_4)[\mathbf{Ar^1}SI_2]$, the S−I and I−I distance are shorter 2.523(3) and longer 3.100(4) Å, respectively. Such a tendency was observed in $(NEt_4)[\mathbf{Ar^1}SI{\cdot}I_2S\mathbf{Ar^1}]$. The sets of S−I and I−I distances were 2.4729(6) and 3.3034(8); 2.5084(19); and 3.1462(9) Å. These reciprocal relationships fit the reported hyperbolic plot of S−I vs I−I distances.[15,21] Intermolecular I···I contact (3.821 Å) between two $(Me_3Si)_3CSI$ molecules was reported; however, such a very weak I···I bond did not affect significantly S−I bond (2.4160(3) Å).[22] On the other hand, the S−I bond (2.4177(12) Å) in $\mathbf{Ar^1}$SI was longer than those of BmtSI (2.386(2) Å)[6] and BpqSI (2.316(4) Å).[13] The C−S distances are in the order $[\mathbf{Ar^1}S]^-$ (1.750(4)) < $\mathbf{Ar^1}$SI (1.761(4)) < $[\mathbf{Ar^1}SI_2]^-$ (1.772(4) Å), indicating that the delocalization of the electron on the sulfur atom was changed from C−S π bond to S−I σ bond by the interaction with electron-deficient iodine atom.

UV−visible Spectra. Absorption spectra of $(NEt_4)[\mathbf{Ar^1}S]$, $\mathbf{Ar^1}$SI, and $(NEt_4)[\mathbf{Ar^1}SI_2]$ in $CHCl_3$ were shown in Figure 3.

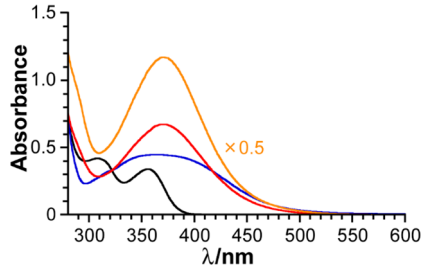

Figure 3. UV−visible spectra of $(NEt_4)[\mathbf{Ar^1}S]$ (1 mM, black), $\mathbf{Ar^1}$SI (1 mM, blue), and $(NEt_4)[\mathbf{Ar^1}SI_2]$ (1 mM, red; 2 mM, half intensity, orange) in $CHCl_3$. Because the absorption of $(NEt_4)[\mathbf{Ar^1}SI_2]$ is dependent on the concentration, orange and red curves show disagreement.

Because the spectra of $(NEt_4)[\mathbf{Ar^1}SI_2]$ are dependent on the concentration, two plots for 1 (red) and 2 mM (orange) are shown. The intensity of the orange curve was reduced by half to make the apparent concentration 1 mM. For the other compounds, the vertical axis equals molar extinction coefficient, $\varepsilon/10^4$ M^{-1} cm^{-1}. As described above, the dissociation constant is about 1 mM; therefore, a half of $(NEt_4)[\mathbf{Ar^1}SI_2]$ is dissociated to $\mathbf{Ar^1}$SI and I^-, suggesting the absorption of the true $(NEt_4)[\mathbf{Ar^1}SI_2]$ without dissociation shows about three-times intensity of the red plot. The absorption of (NEt_4)-$[\mathbf{Ar^1}SI_2]$ showed a broad signal at about 370 nm, which is similar to that of $\mathbf{Ar^1}$SI in $CHCl_3$. The former was a slightly sharp but thermodynamic analysis was difficult because of the difficulty to separate signals and limited solubility of NEt_4I in $CHCl_3$.

In order to attempt the direct observation of the intermediate, the oxidation reaction of $\mathbf{Ar^1}$SI by I_2 was monitored by absorption spectra. The spectral changes are

DOI: 10.1021/acs.joc.7b00160
J. Org. Chem. 2017, 82, 2187−2192

shown in Figure S6 along with the related spectra. To a solution of $(NEt_4)[\mathbf{Ar^1}S]$ (2 mM) was added dropwise a purple solution of I_2 in $CHCl_3$. The characteristic absorption at 512 nm in $CHCl_3$ was disappeared immediately. The addition of 0.5 equimolar I_2 resulted broad absorption due to the formation of $\mathbf{Ar^1}SI$ and/or $[\mathbf{Ar^1}SI_2]^-$ and the residual absorption of $(NEt_4)[\mathbf{Ar^1}S]$ was observed at 318 nm. At the initial stage, the main reaction was probably yielded 0.5 $(NEt_4)[\mathbf{Ar^1}SI_2]$ (1 mM). After addition of total 1.0 equimolar I_2, intense peak raised at 366 nm suggesting the formation of $(NEt_4)[I_3]$ (<1 mM). These results suggested that at least two stages were present. At the initial stage, i.e., at low concentration of I^-, I_2 was reacted with $[\mathbf{Ar^1}S]^-$ mainly to produce $\mathbf{Ar^1}SI$ and I^- or $[\mathbf{Ar^1}SI_2]^-$. At next stage, i.e., at adequate concentration of I^-, I_2 was reacted with I^- rather than $[\mathbf{Ar^1}S]^-$ to form $[I_3]^-$. The anionic $[I_3]^-$ probably could not react with anionic $[\mathbf{Ar^1}S]^-$ in a similar mechanism as shown in eq 6. Such reactions probably occurred in less polar solvents like $CHCl_3$. In polar solvents, $[I_3]^-$ should be more easily dissociate to reproduce I_2. In the synthesis of $\mathbf{Ar^1}SI$, K^+ salt, $K[\mathbf{Ar^1}S]$, and I_2 reacted in acetonitrile/toluene. In this reaction system, insoluble KI was separated out without formation of KI_3, resulting in almost quantitative yield.

Theoretical Calculations. The structural and spectroscopic data indicate that NH···S hydrogen bonds elongate the S−I bond in RSI, but stabilize the I−I bond in $[RSI_2]^-$. To confirm these findings, theoretical calculations using density functional theory (DFT) were performed. Two simplified model compounds $[\mathbf{Ar^3}SI_2]^-$ and $[Me_2C_6H_3SI_2]^-$ shown in Figure 4 were used to evaluate the contribution of the hydrogen

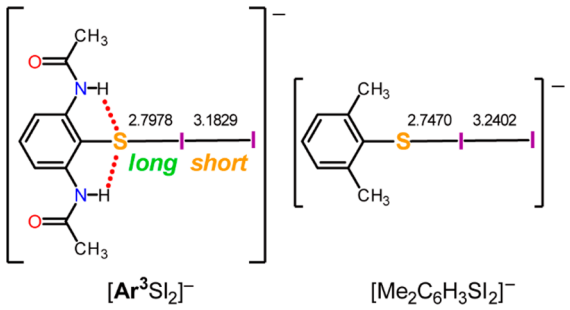

Figure 4. Model compounds for DFT calculations along with the geometrically optimized distances (Å).

bonds separately from the other factors, e.g., bulkiness. An imaginary compound $[BmtSI_2]^-$ was also used for comparison. The optimized geometrical parameters are shown in Table S3. Obviously, NH···S hydrogen bonds shorten C−S and I−I bonds and elongate S−I bond. The replacement of $\mathbf{Ar^1}$ with $\mathbf{Ar^3}$ and Bmt with $Me_2C_6H_3$ afforded similar values, indicating that the bulkiness or steric hindrance of the substituents less affected the bond distances. The small differences are probably caused by the weak electron-donating character of the aromatic groups. In the actual case, bulkiness is necessary to prevent the intermolecular reaction producing disulfide. The electronically unfavorable hydrogen-bonded S−I bond in $\mathbf{Ar^1}SI$ is probably stabilized by the steric effect. The effects of the NH···S hydrogen bond are illustrated in Figure 4. The stabilization of S−I−I bond was evaluated by natural bond orbital (NBO) analysis.[23,24] The SI−I bond is regarded as CT from the lone pair of the terminal I (n_I), i.e., filled p orbital, to the vacant antibonding S−I σ bond (σ^*_{SI}). The second-order perturbative estimates of $n_I \rightarrow \sigma^*_{SI}$ interaction provided the required stabilization energy. The calculated values (in units of kcal mol^{-1}) follow the order $[\mathbf{Ar^3}SI_2]^-$ (64.14) > $[\mathbf{Ar^1}SI_2]^-$ (57.59) > $[Me_2C_6H_3SI_2]^-$ (47.37). As mentioned above, the bulky Ar_3C group acts as an electron-donating group, resulting in a weaker hydrogen bond and less stabilization energy than $[\mathbf{Ar^3}SI_2]^-$.

As described in the UV-visible Spectra Section, (NEt_4)-$[\mathbf{Ar^1}SI_2]$ presumably exhibits intense ($\varepsilon \sim 2 \times 10^4$ M^{-1} cm^{-1}) without the dissociation at ~370 nm, which is close to the absorption maximum of $\mathbf{Ar^1}SI$ but the ε is four to five times larger. In order to assign the absorption band, time-dependent (TD) DFT calculations were performed. The calculated transition bands and molecular orbitals (MOs) are shown in Figure S7. The results indicated the bulky Ar_3C group did not affect significantly MOs. The HOMO of $[\mathbf{Ar^1}SI_2]^-$ is regarded as the combination of nonbonding orbital of the terminal I and the HOMO of $[\mathbf{Ar^1}S]^-$ anion. The LUMO is essentially antibonding orbital of S−I−I array. The first absorption band, i.e., the lowest energy excitation, predominantly reflects the transition from the terminal I^- to the σ^*-type S−I−I array, which is closely related to the stabilization of S−I−I bond as described above. The moiety reminds us $[I-I-I]^-$ anion showing a similar intense absorption at 363 nm (Figure S6) and their MOs also resemble the corresponding ones, nonbonding orbital (n_I) and antibonding orbital (σ^*_{I-I-I}) (Figure S7). For $\mathbf{Ar^1}SI$, the absorption band is the transition from nonbonding orbitals of the terminal I to LUMO that contains antibonding σ^* orbital of S−I.

CONCLUSIONS

The NH···S hydrogen bond decreases the electron density on sulfur atom and the donation to the electron-deficient iodine, thus increasing the electron-acceptability of iodine from iodide anion. The complete mechanism is shown in Figure 5. NH···S

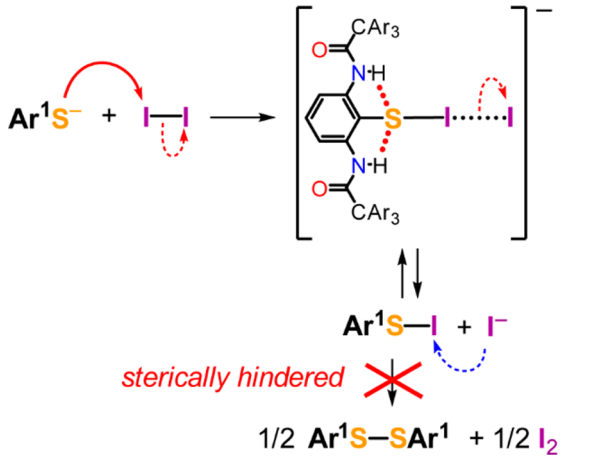

Figure 5. Stabilization of I···I bond by NH···S hydrogen bonds. The curved arrows indicate the electron transfer in forward (red) and backward (blue) reactions.

hydrogen bonds are widely found in metalloproteins and enzymes. In our model complexes of molybdoenzymes, benzenedithiolate ligand showed a partial dithioketone character, which was effectively stabilized by the NH···S hydrogen bond.[25] In this case, $[\mathbf{Ar^1}S]^-$ showed a partial thione-like character, achieving a stable C−S−I−I bond such as a C═S···I−I bond known for thiones. If necessary, cysteine residues ($RS^{-II}H$) are modified or oxidized to disulfide

DOI: 10.1021/acs.joc.7b00160
J. Org. Chem. 2017, 82, 2187−2192

$[(RS^{-I})_2]$, sulfenic acid (RS^0OH), sulfinic acid ($RS^{II}O_2H$), etc. in biological systems.[26] The oxidation state of S should be regulated by certain mechanisms. The NH···S hydrogen bonds probably contribute to the regulation along with the conformational change of proteins depending on the environment.

EXPERIMENTAL SECTION

Materials. All solvents were dried and distilled before use and reaction was carried out under argon atmosphere using Schlenk technique. Ar_3CCOCl (Ar- = *t*-BuC_6H_4-) and bis(2,6-diaminophenyl) disulfide were prepared by the literature procedure.[4,10,27]

2,6-(Ar_3CCONH)$_2C_6H_3SSC_6H_3$-2′-NH_2-6′-NHCOAr_3. To a solution of bis(2,6-diaminophenyl) disulfide (170.8 mg, 0.614 mmol) and NEt_3 (1.0 mL, 7.1 mmol) in CH_2Cl_2 (4 mL) was added Ar_3CCOCl (1.12 g, 2.36 mmol) in CH_2Cl_2 (6 mL) cooling in an ice bath. The mixture was refluxed for 24 h to give a brown solution. The solution was concentrated to dryness under reduced pressure. The resulting residue was extracted with ethyl acetate. The solution was washed with 4% $NaHCO_3$ aq., sat. NaCl aq., 0.06% HCl aq., and sat. NaCl aq., successively. The organic layer was dried over Na_2SO_4 and concentrated under reduced pressure to give a yellow residue. This residue was dissolved in a small volume of ethyl acetate. The addition of hot ethanol gave light yellow powder, which was collected and washed ethanol and dried *in vacuo*. Yield: 451 mg (46%). ^{1}H NMR (500 MHz, $CDCl_3$) 8.59 (s, 1H, NH), 8.04 (s, 2H, NH) 7.90 (br, 1H, 3(5)-H), 7.77 (br, 2H, 4,5(3)-H), 7.23 (m, 12H, Ar), 7.14 (m, 6H, Ar), 7.06 (m, 18H, Ar), 6.82 (t, 1H, 4′-H), 5.97 (dd, 1H, 3′-H), 3.51 (s, 2H, NH_2), 1.25 (s, 54H, *t*-Bu), 1.22 (s, 27H, *t*-Bu).

2,6-(Ar_3CCONH)$_2C_6H_3SSC_6H_3$-2′-NHCO-t-Bu-6′-NHCOAr_3 (Ar^1SSAr^2). To a solution of 2,6-(Ar_3CCONH)$_2C_6H_3SSC_6H_3$-2′-NH_2-6′-NHCOAr_3 (149 mg, 0.093 mmol) and NEt_3 (1.45 mL, 10.4 mmol) in CH_2Cl_2 (1 mL) was added a solution of pivaloyl chloride (1.07 M, 1.5 mL, 1.6 mmol). This mixture was refluxed for 24 h to give a pale yellow solution. The solution was removed in vacuo, extracted by toluene and washed with 4% $NaHCO_3$ aq., sat. NaCl aq., 2% HCl aq., sat. NaCl aq., successively. The organic layer was dried over Na_2SO_4 and concentrated under reduced pressure to give pale yellow residue. This residue was recrystallized from ethyl acetate to give colorless plate crystal. Yield: 74.6 mg (48%). Recrystallization from 1,4-dioxane gave colorless columns. Anal. Calcd for $C_{113}H_{136}O_4N_4S_2$·(1,4-dioxane): C, 79.55; H, 8.22; N, 3.17. Found: C, 79.71; H, 8.21, N, 3.16. ^{1}H NMR ($CDCl_3$, Figure S8): δ 8.54, 8.46 (br, 4H, NH), 7.6–6.8 (br, 42H, aromatic signals), 1.23 (s, 81H, *t*-Bu of Ar), 0.97 (br, 9H, *t*-Bu). $^{13}C\{^1H\}$ NMR ($CDCl_3$): δ 172.8, 172.6, 149.7, 149.6, 140.7, 140.0, 131.6, 130.2, 130.1, 125.0, 117.3, 34.40, 34.39, 34.38, 31.38, 31.37, 31.35, 27.4.

(NEt_4)[Ar^1S]. To a suspension of Ar^1SSAr^2 (737 mg, 0.439 mmol) in a mixture of toluene (1.3 mL) and ethanol (20 mL) was added NEt_4BH_4 (181 mg, 1.25 mmol) and stirred overnight to afford white precipitates, which were collected with centrifugation, washed by MeOH, and dried under reduced pressure to give white powder. Yield: 426 mg (85%). Recrystallization from toluene/*n*-hexane containing a drop of acetonitrile afforded colorless blocks, which are appropriate to X-ray analysis. The crystal solvents were easily removed under reduced pressure and replaced by water molecules. Anal. Calcd for $C_{78}H_{103}N_3O_2S$·H_2O: C, 80.43; H, 9.09; N, 3.61. Found: C, 80.36; H, 8.97; N, 3.69. ^{1}H NMR ($CDCl_3$, Figure S9): δ 10.03 (s, 2H, NH), 7.93 (d, J = 8.1 Hz, 2H, 3,5-H), 7.28 (m, 12H, Ar), 7.25(m, 12H, Ar), 6.61 (t, J = 8.4 Hz, 1H, 4-H), 2.54 (q, J = 7.3 Hz, 8H, CH_2), 1.28 (s, 54H, *t*-Bu), 0.83 (t, J = 7.3 Hz, 12H, CH_3). $^{13}C\{^1H\}$ NMR ($CDCl_3$): δ 172.4, 149.9, 149.0, 140.6, 140.2, 130.4, 125.0, 122.9, 108.1, 66.0, 52.9, 34.6, 31.5, 8.0.

(NEt_4)[Ar^1SI·I_2SAr^1]. To a solution of (NEt_4)[Ar^1S] (83.1 mg, 72.5 μmol) in 5.0 mL of toluene was added dark purple suspension of I_2 (20.3 mg, 80.1 μmol) in 2.0 mL of toluene to give orange suspension. After stirred overnight, the insoluble reddish brown precipitates were removed by centrifugation. The supernatant was concentrated to dryness under reduced pressure, washed with *n*-hexane. The resulting solid was crystallized from toluene to give reddish orange blocks and colorless microcrystals. The residual crystals were extracted with toluene and recrystallized from hot toluene to afford reddish orange blocks, which were characterized to be (NEt_4)[Ar^1SI·I_2SAr^1] by X-ray analysis, and pale yellow needles.

K[Ar^1S]. To a pale yellow suspension of Ar^1SSAr^2 (735.1 mg, 0.44 mmol) in a mixture of toluene (2.5 mL) and ethanol (6.0 mL) was added KBH_4 (83.7 mg, 1.55 μmol) and stirred overnight to give white suspension. The reaction mixture was concentrated under reduced pressure. The white precipitate was washed with methanol to give white powder. Yield: 432.5 mg, 94%. This compound was used for the following reaction without further purification. ^{1}H NMR (CD_3CN, Figure S10): δ 10.24 (s, 2H, NH), 7.90 (d, J = 8.1 Hz, 2H, 3,5-H), 7.32 (m, 12H, Ar), 7.25 (m, 12H, Ar), 6.51 (t, J = 8.1 Hz, 1H, 4-H), 1.28 (s, 54H, *t*-Bu). ^{1}H NMR ($CDCl_3$): δ 9.24 (s, 2H, NH), 7.37 (d, 2H, Ar), 7.25 (m, 24H, Ar), 6.48 (t, 1H, Ar), 1.27 (s, 54H, *t*-Bu). $^{13}C\{^1H\}$ NMR (CD_3CN): δ 171.9, 150.1, 142.7, 139.2, 137.4, 131.4, 125.5, 116.9, 112.7, 69.0, 35.0, 31.7. HRMS (ESI/Orbitrap): Calcd for Ar^1S^-: m/z 1015.6175. Found: 1015.6190.

Ar^1SI. To a colorless solution of K[Ar^1S] (361 mg, 342 μmol) in toluene (3.0 mL) and acetonitrile (2.0 mL) was added I_2 (93 mg, 365 μmol) in toluene (1.2 mL) at 0 °C to give red solution and yellow precipitates. After stirring overnight at 65 °C, the solvents were removed under reduced pressure to give a red powder. The crude product was extracted with hot toluene. The resulting red solution was concentrated to dryness under reduced pressure. The residual orange crystalline powder was washed by 1,2-dimethoxyethane (DME), and dried under reduced pressure to give orange powder. Recrystallization from hot DME afforded orange plates, which were used for X-ray analysis. Yield: 346.7 mg, 89%. ^{1}H NMR ($CDCl_3$, Figure S11): δ 8.96 (s, 2H, NH), 8.37 (d, J = 8.5 Hz, 2H, 3,5-H), 7.42 (t, J = 8.5 Hz, 1H, 4-H), 7.32 (m, 12H, Ar), 7.24 (m, 12H, Ar), 1.30 (s, 54H, *t*-Bu). $^{13}C\{^1H\}$ NMR ($CDCl_3$): δ 172.8, 149.9, 142.8, 140.2, 130.4, 125.1, 115.4, 107.6, 68.3, 34.6, 31.5. Anal. Calcd for $C_{70}H_{83}N_2O_2S$·0.5($C_4H_{10}O_2$)·2(H_2O): C, 70.62; H, 7.57; N, 2.29. Found: C, 70.83; H, 7.50; N, 2.28. IR (KBr): 3329 (ν_{NH}), 1689 ($\nu_{C=O}$) cm^{-1}.

(NEt_4)[Ar^1SI_2]. To a solution of Ar^1SI (12.0 mg, 10.3 μmol) in $CHCl_3$ (1 mL) was added NEt_4I (2.63 mg, 10.3 μmol) at room temperature. The orange solution was allowed to evaporate gradually at room temperature for several days. Clear orange blocks crystallized, which were suitable for X-ray analysis. After the supernatant was removed, the crystals were dried under reduced pressure. The product lost the crystal solvents and resulted in an orange powder. Yield: 9.6 mg (66%). ^{1}H NMR ($CDCl_3$): δ 9.13 (s, 2H, NH), 8.27 (d, 2H, 3,5-H), 7.34 (m, 12H, Ar), 7.26 (t, 1H, 4-H), 7.25 (m, 12H, Ar), 3.18 (q, 8H, CH_2), 1.30 (s, 54H, *t*-Bu), 1.20 (t, 12H, CH_3). $^{13}C\{^1H\}$ NMR ($CDCl_3$, Figure S12): δ 173.2, 149.7, 141.2, 140.1, 130.4, 125.0, 115.08, 115.05, 68.0, 53.1, 34.4, 31.4, 8.0. Anal. Calcd for $C_{78}H_{103}I_2N_3O_2S$: C, 66.89; H, 7.41; N, 3.00. Found: C, 67.03; H, 7.57; N, 2.95.

Physical Measurements. Proton nuclear magnetic resonance spectroscopy (^{1}H NMR) spectra were obtained on a JEOL ECA-500, ECA-400WB, ECS-400 spectrometer, using $CDCl_3$, CD_3CN, and toluene-d_8 solution at 303 K. High-resolution electrospray ionization mass spectroscopy (HRMS-ESI) measurements were carried out with a Thermo Fisher Scientific LTQ Orbitrap XL using MeCN/THF = 1:1 solution in positive and negative modes. Infrared (IR) spectroscopic measurements were done on a Jasco FT/IR-4000 spectrometer. UV–visible absorption spectra were recorded using a SHIMADZU UV-3100PC spectrometer using a quartz cell with 1 mm optical path length.

X-ray Analysis. Each single crystal of (NEt_4)[Ar^1S]·1.75CH_3CN, (NEt_4)[Ar^1SI·I_2Ar^1]·8(toluene), [Ar^1SI]·DME, (NEt_4)[Ar^1SI_2]·5$CHCl_3$ was selected carefully and mounted on MicroMount 200 μm with Nujol, which was frozen immediately in a stream of cold nitrogen at 200 K. Data collection was made on a Rigaku RAPID II Imaging Plate area detector with Mo Kα radiation (0.71075 Å) using MicroMax-007HF microfocus rotating anode X-ray generator and VariMax-Mo optics. The structure was solved by direct methods (SIR92,[28] SHELXS[29]) and expanded Fourier techniques using SHELXL-2014/7 and SHELXL-2016/6.[29] Non-hydrogen atoms

DOI: 10.1021/acs.joc.7b00160
J. Org. Chem. 2017, 82, 2187–2192

were refined anisotropically. The H atoms were generated by the riding and rotating model in SHELXL-97.[29]

■ ASSOCIATED CONTENT

Supporting Information

The Supporting Information is available free of charge on the ACS Publications website at DOI: 10.1021/acs.joc.7b00160.

X-ray crystallographic data for $(NEt_4)[\mathbf{Ar^1}S]$, $(NEt_4)[\mathbf{Ar^1}SI{\cdot}I_2\mathbf{SAr^1}]$, $[\mathbf{Ar^1}SI]$, and $(NEt_4)[\mathbf{Ar^1}SI_2]$; geometrical parameters of observed and optimized structures; ^1H NMR spectra of mixtures of $\mathbf{Ar^1}SI$ and NEt_4I; analysis of the dissociation of $(NEt_4)[\mathbf{Ar^1}SI_2]$; UV−visible spectra; MOs; ^1H and ^{13}C NMR spectra; and details of computational methods and results (PDF)

X-ray crystallographic data for $(NEt_4)[\mathbf{Ar^1}S]$, $(NEt_4)[\mathbf{Ar^1}SI{\cdot}I_2\mathbf{SAr^1}]$, $[\mathbf{Ar^1}SI]$, and $(NEt_4)[\mathbf{Ar^1}SI_2]$ (CIF)

■ AUTHOR INFORMATION

Corresponding Author

*E-mail: tokamura@chem.sci.osaka-u.ac.jp.

ORCID

Taka-aki Okamura: 0000-0002-9005-4015

Notes

The authors declare no competing financial interest.

■ ACKNOWLEDGMENTS

This work was supported by JSPS KAKENHI Grant Number JP 26410072.

■ REFERENCES

(1) Fraenkel-Conrat, H. *J. Biol. Chem.* **1955**, *217*, 373−381.
(2) Rheinboldt, H.; Motzkus, E. *Ber. Dtsch. Chem. Ges. B* **1939**, *72*, 657−667.
(3) Danehy, J. P.; Oester, M. Y. *J. Org. Chem.* **1967**, *32*, 1491−1495.
(4) Danehy, J. P.; Egan, C. P.; Switalski, J. *J. Org. Chem.* **1971**, *36*, 2530−2534.
(5) deLeeuw, D. L.; Musker, W. K.; Doi, J. T. *J. Org. Chem.* **1982**, *47*, 4860−4864.
(6) Goto, K.; Holler, M.; Okazaki, R. *Chem. Commun.* **1998**, 1915−1916.
(7) Hasenaka, Y.; Okamura, T.; Tatsumi, M.; Inazumi, N.; Onitsuka, K. *Dalton Trans.* **2014**, *43*, 15491−15502.
(8) Okamura, T.; Furuya, R.; Onitsuka, K. *J. Am. Chem. Soc.* **2014**, *136*, 14639−14641.
(9) Okamura, T.; Yamada, T.; Hasenaka, Y.; Yamashita, S.; Onitsuka, K. *Eur. J. Inorg. Chem.* **2016**, *2016*, 2952−2961.
(10) Ueyama, N.; Okamura, T.; Yamada, Y.; Nakamura, A. *J. Org. Chem.* **1995**, *60*, 4893−4899.
(11) CCDC 1508518 ($(NEt_4)[\mathbf{Ar^1}S]$), 1508519 ($(NEt_4)[\mathbf{Ar^1}SI{\cdot}I_2\mathbf{SAr^1}]$), 1508520 ($[\mathbf{Ar^1}SI]$), and 1508521 ($(NEt_4)[\mathbf{Ar^1}SI_2]$).
(12) Chadwick, S.; Englich, U.; Ruhlandt-Senge, K.; Watson, C.; Bruce, A. E.; Bruce, M. R. M. *J. Chem. Soc., Dalton Trans.* **2000**, 2167−2173.
(13) Goto, K.; Yamamoto, G.; Tan, B.; Okazaki, R. *Tetrahedron Lett.* **2001**, *42*, 4875−4877.
(14) Aragoni, M. C.; Arca, M.; Devillanova, F. A.; Garau, A.; Isaia, F.; Lippolis, V.; Verani, G. *Coord. Chem. Rev.* **1999**, *184*, 271−290.
(15) Herbstein, F. H.; Schwotzer, W. *J. Am. Chem. Soc.* **1984**, *106*, 2367−2373.
(16) Freeman, F.; Ziller, J. W.; Po, H. N.; Keindl, M. C. *J. Am. Chem. Soc.* **1988**, *110*, 2586−2591.
(17) Tretiakov, M.; Shermolovich, Y. G.; Singh, A. P.; Samuel, P. P.; Roesky, H. W.; Niepötter, B.; Visscher, A.; Stalke, D. *Dalton Trans.* **2013**, *42*, 12940−12946.
(18) Blake, A. J.; Gould, R. O.; Radek, C.; Schröder, M. *J. Chem. Soc., Chem. Commun.* **1993**, 1191−1193.
(19) Mancini, A.; Aragoni, M. C.; Bricklebank, N.; Castellano, C.; Demartin, F.; Isaia, F.; Lippolis, V.; Pintus, A.; Arca, M. *Chem. - Asian J.* **2013**, *8*, 639−647.
(20) van Bolhuis, F.; Koster, P. B.; Migchelsen, T. *Acta Crystallogr.* **1967**, *23*, 90−91.
(21) Deplano, P.; Ferraro, J. R.; Mercuri, M. L.; Trogu, E. F. *Coord. Chem. Rev.* **1999**, *188*, 71−95.
(22) Wismach, C.; Jones, P. G.; du Mont, W.-W.; Mugesh, G.; Papke, U.; Linden, H. B.; Arca, M.; Lippolis, V. *Eur. J. Inorg. Chem.* **2014**, *2014*, 1399−1406.
(23) Weinhold, F.; Landis, C. R. *Valency and Bonding. A Natural Bond Orbital Donor-Acceptor Perspective*; Cambridge University Press: Cambridge, 2005.
(24) Weinhold, F.; Landis, C. R. *Discovering Chemistry with Natural Bond Orbitals*; John Wiley & Sons, Inc.: Hoboken, 2012.
(25) Okamura, T.; Tatsumi, M.; Omi, Y.; Yamamoto, H.; Onitsuka, K. *Inorg. Chem.* **2012**, *51*, 11688−11697.
(26) Gupta, V.; Carroll, K. S. *Biochim. Biophys. Acta, Gen. Subj.* **2014**, *1840*, 847−875.
(27) Okamura, T.; Ushijima, Y.; Omi, Y.; Onitsuka, K. *Inorg. Chem.* **2013**, *52*, 381−394.
(28) Altomare, A.; Burla, M. C.; Camalli, M.; Cascarano, M.; Giacovazzo, C.; Guagliardi, A.; Polidori, G. *J. Appl. Crystallogr.* **1994**, *27*, 435.
(29) Sheldrick, G. M. *Acta Crystallogr., Sect. A: Found. Crystallogr.* **2008**, *64*, 112−122.

DOI: 10.1021/acs.joc.7b00160
J. Org. Chem. 2017, 82, 2187−2192